

**GREEN ZINC OXIDE-BASED
PHOTOCATALYSTS:
PREPARATION, CHARACTERIZATION AND
PHOTOCATALYTIC STUDY FOR THE
DEGRADATION OF DYES UNDER VISIBLE
LIGHT IRRADIATION**

FATIN HAZIRAH BINTI ABDULLAH

UNIVERSITI SAINS MALAYSIA

2023

**GREEN ZINC OXIDE-BASED
PHOTOCATALYSTS:
PREPARATION, CHARACTERIZATION AND
PHOTOCATALYTIC STUDY FOR THE
DEGRADATION OF DYES UNDER VISIBLE
LIGHT IRRADIATION**

by

FATIN HAZIRAH BINTI ABDULLAH

**Thesis submitted in fulfilment of the requirements
for the degree of
Doctor of Philosophy**

August 2023

ACKNOWLEDGEMENT

In the name of Allah, the Most Gracious, the Most Merciful

Alhamdulillah, all praises to Allah the Almighty for His blessings and the strength, courage, and perseverance He has given me to complete my PhD journey. I would like to express my utmost appreciation to my supervisor, Associate Professor Dr. Noor Hana Hanif Abu Bakar for her continuous support, advices, and insightful comments throughout the period of my study. I would also like to thank Professor Dr. Mohamad Abu Bakar for his immense knowledge, inspiration, and motivation. I am grateful for their patience and guidance. May Allah preserve them upon goodness.

I would like to acknowledge Universiti Sains Malaysia (USM) for awarding me the prestigious USM Fellowship as well as providing the financial support through Research University Individual grant (1001/PKIMIA/8011071). I would like to extend my gratitude to the technical and administrative staff of School of Chemical Sciences, School of Physics, Centre for Global Archeological Research, Science and Engineering Research Centre, and Institute of Postgraduate Studies for their kind assistance and excellent services. My appreciation also goes to my lab members, friends, and lecturers for their kind help, moral support, and encouragement during my study.

Most of all, I dedicate my thesis to my dearest mother, Zaimun binti Roslan, my loving late father, Abdullah bin Baharom, and my wonderful sister, Ili Haziqah binti Abdullah. Thank you very much for the love, care, patience, and support you have shown me throughout my PhD journey and my entire life. Words cannot express how grateful I am for all of the sacrifices that you have made on my behalf. I hope I have made you proud. May Allah bless you abundantly in this life and the Hereafter.

TABLE OF CONTENTS

ACKNOWLEDGEMENT	ii
TABLE OF CONTENTS	iii
LIST OF TABLES	x
LIST OF FIGURES	xii
LIST OF SYMBOLS	xviii
LIST OF ABBREVIATIONS	xx
ABSTRAK	xxiii
ABSTRACT	xxv
CHAPTER 1 INTRODUCTION	1
1.1 Background	1
1.2 Problem statements	3
1.3 Research objectives	5
1.4 Significance of study	5
1.5 Scope of study	6
1.6 Thesis outline	7
CHAPTER 2 LITERATURE REVIEW	9
2.1 Dyes as organic contaminants	9
2.2 Fundamental of heterogenous photocatalysis	14
2.2.1 Photocatalyst and its characteristics	15
2.2.2 Metal oxide semiconductor photocatalyst	16
2.2.3 Principle and mechanism of photocatalysis	18
2.3 Properties and features of zinc oxide (ZnO)	20
2.3.1 ZnO structure and classification	20
2.3.2 ZnO shape and size control	26

2.4	Fabrication of ZnO	29
2.4.1	Physical method	29
2.4.2	Chemical method	30
2.4.3	Biosynthesis or green method	31
2.5	Modification of ZnO	37
2.5.1	Metal doping	37
2.5.2	Semiconductor coupling	41
2.6	Immobilization of ZnO on polymeric materials.....	44
2.6.1	Synthetic polymers.....	45
2.6.2	Natural polymers.....	47
2.7	Natural rubber (NR) and polyvinylpyrrolidone (PVP) polymers	49
2.8	Bio-inspired nanomaterials for photocatalytic application using renewable and biodegradable resources	51
CHAPTER 3 EXPERIMENTAL		54
3.1	Materials.....	54
3.2	Synthesis of ZnO nanoparticles	54
3.2.1	Preparation of banana peel (BP) extract	54
3.2.2	Biosynthesis of ZnO nanoparticles and optimization of synthesis parameters	55
3.2.3	Chemical synthesis of ZnO nanoparticles.....	56
3.3	Fabrication of ZnO-based nanocomposites.....	57
3.3.1	Preparation of natural rubber-polyvinylpyrrolidone (NR-PVP) film.....	57
3.3.2	Preparation of impregnated-natural rubber-polyvinylpyrrolidone/zinc oxide (i-NR-PVP/ZnO) film by impregnation method	57
3.3.3	Preparation of strewn-natural rubber-polyvinylpyrrolidone/zinc oxide (s-NR-PVP/ZnO) film by strewn method	58
3.4	Characterizations.....	58

3.4.1	X-ray diffraction (XRD)	58
3.4.2	Fourier transform infrared spectroscopy (FTIR)	59
3.4.3	Scanning electron microscopy-energy dispersive X-ray spectroscopy (SEM-EDX)	60
3.4.4	Ultraviolet-visible diffuse reflectance spectroscopy (UV-Vis DRS).....	60
3.4.5	Photoluminescence spectroscopy (PL)	61
3.4.6	Transmission electron microscopy (TEM)	61
3.4.7	Nitrogen adsorption-desorption (NAD).....	62
3.4.8	X-ray photoelectron spectroscopy (XPS)	62
3.4.9	Thermogravimetric analysis (TGA).....	62
3.4.10	Point of zero charge (pH_{pzc})	63
3.4.11	Dynamic light scattering (DLS).....	63
3.4.12	Total organic carbon (TOC).....	64
3.5	Photocatalytic studies using suspended ZnO nanoparticles.....	64
3.5.1	Experimental setup.....	64
3.5.2	Evaluation of photocatalytic reactions.....	66
3.5.3	Evaluation on the effect of initial concentration of methylene blue (MB).....	66
3.5.4	Evaluation on the effect of catalyst loading.....	67
3.5.5	Evaluation on the effect of solution pH and irradiation time.....	67
3.5.6	Scavenging test	67
3.5.7	Reusability studies	68
3.5.8	Photocatalytic removal of other dyes by ZnO nanoparticles	68
3.6	Photocatalytic studies using immobilized ZnO nanocomposite films.....	68
3.6.1	Evaluation on the effect of ZnO loading.....	68
3.6.2	Evaluation on the effect of type and intensity of light.....	69
3.6.3	Evaluation on the effect of solution pH	69
3.6.4	Scavenging test	69

3.6.5	Reusability studies	70
3.6.6	Photocatalytic removal of other dyes by ZnO nanocomposite films	70
3.7	Outline of experimental approach	71
CHAPTER 4 RESULTS AND DISCUSSION		
OPTIMIZATION OF SYNTHESIS PARAMETERS OF BIOSYNTHESIZED ZnO NANOPARTICLES AND ITS PHOTOCATALYTIC ACTIVITY		
72		
4.1	Overview	72
4.2	Characterization of green ZnO synthesized at different pH.....	73
4.2.1	Ultraviolet-visible diffuse reflectance spectroscopy (UV-Vis DRS) analysis.....	73
4.2.2	Fourier transform infrared spectroscopy (FTIR) analysis.....	75
4.2.3	X-ray diffraction (XRD) analysis	77
4.2.4	Scanning electron microscopy (SEM) analysis	80
4.2.5	Photoluminescence spectroscopy (PL) analysis	82
4.3	Effect of synthesis pH of ZnO on the removal of MB.....	84
4.4	Optimization of other synthesis parameters	85
4.4.1	Effect of amount of BP extract	86
4.4.2	Effect of concentration of zinc acetate dihydrate.....	87
4.4.3	Effect of synthesis time.....	88
4.4.4	Effect of temperature	89
4.5	Summary	91
CHAPTER 5 RESULTS AND DISCUSSION		
CHARACTERIZATIONS AND PHOTOCATALYTIC ACTIVITIES OF ZnO NANOPARTICLES PREPARED VIA CHEMICAL AND ENVIRONMENTALLY-BENIGN METHODS		
92		
5.1	Overview	92
5.2	Characteristics of ZnO photocatalysts	93
5.2.1	X-ray diffraction (XRD) analysis	93

5.2.2	Fourier transform infrared spectroscopy (FTIR) analysis.....	95
5.2.3	Scanning electron microscopy-energy dispersive X-ray spectroscopy (SEM-EDX) analysis	97
5.2.4	Transmission electron microscopy (TEM) analysis.....	100
5.2.5	Nitrogen adsorption-desorption (NAD) analysis	102
5.2.6	Dynamic light scattering (DLS) analysis	104
5.2.7	Ultraviolet-visible diffuse reflectance spectroscopy (UV-Vis DRS) analysis.....	106
5.2.8	Photoluminescence spectroscopy (PL) analysis	108
5.2.9	X-ray photoelectron spectroscopy (XPS) analysis.....	110
5.2.10	Point of zero charge (pH_{pzc})	112
5.3	Photocatalytic activity of green ZnO photocatalyst.....	113
5.3.1	Effect of initial concentration of MB.....	113
5.3.2	Effect of catalyst loading	114
5.3.3	Effect of pH and irradiation time	115
5.3.4	Comparison of photocatalytic performances of photocatalysts ...	118
5.3.5	Reusability studies	120
5.3.6	Scavenging test	122
5.3.7	Proposed photodegradation mechanism.....	123
5.3.8	Mineralization studies	125
5.3.9	Photocatalytic removal of other dyes.....	126
5.3.10	Comparative studies with previous works	128
5.4	Summary	134
 CHAPTER 6 RESULTS AND DISCUSSION		
PREPARATION AND CHARACTERIZATIONS OF IMPREGNATED- AND STREWN-NATURAL RUBBER-POLYVINYLPIRROLIDONE/ZINC OXIDE BIO-NANOCOMPOSITES		
135		
6.1	Overview	135
6.2	Preparation of i-NR-PVP/ZnO and s-NR-PVP/ZnO composite films.....	136

6.3	Characteristics of i-NR-PVP/ZnO and s-NR-PVP/ZnO composite films.....	137
6.3.1	X-ray diffraction (XRD) analysis	137
6.3.2	Fourier transform infrared spectroscopy (FTIR) analysis.....	139
6.3.3	Scanning electron microscopy-energy dispersive X-ray spectroscopy (SEM-EDX) analysis	143
6.3.4	Ultraviolet-visible diffuse reflectance spectroscopy (UV-Vis DRS) analysis.....	148
6.3.5	Photoluminescence spectroscopy (PL) analysis	152
6.3.6	Thermogravimetric analysis (TGA).....	154
6.3.7	Point of zero charge (pH_{pzc}).....	158
6.4	Summary	160
CHAPTER 7 RESULTS AND DISCUSSION		
PHOTOCATALYTIC ACTIVITIES OF IMPREGNATED- AND STREWN-NATURAL RUBBER-POLYVINYLPIRROLIDONE/ZINC OXIDE BIO-NANOCOMPOSITES		
161		
7.1	Overview	161
7.2	Photocatalytic activities and kinetic studies of i-NR-PVP/ZnO and s-NR-PVP/ZnO films.....	162
7.2.1	Effect of ZnO loading	162
7.2.2	Effect of type and intensity of light	171
7.2.3	Effect of pH.....	175
7.2.4	Scavenging test	179
7.2.5	Proposed photodegradation mechanism.....	181
7.2.6	Reusability studies	186
7.2.7	Mineralization studies	189
7.2.8	Photocatalytic removal of other dyes.....	189
7.2.9	Comparative studies with previous works	192
7.3	Summary	193

CHAPTER 8	CONCLUSIONS AND RECOMMENDATIONS	194
8.1	Conclusions	194
8.2	Recommendations for future works	196
REFERENCES.....		197
LIST OF PUBLICATIONS AND PRESENTATIONS		

LIST OF TABLES

		Page
Table 2.1	Classification of dyes (Akbari <i>et al.</i> , 2002; Kaykhahi <i>et al.</i> , 2018).	10
Table 2.2	The advantages and disadvantages of various treatment technologies for dye removal from water (Solayman <i>et al.</i> , 2023; Srivatsav <i>et al.</i> , 2020).	13
Table 2.3	The band gap energies of various semiconductor photocatalysts (Karthikeyan <i>et al.</i> , 2020; Zhang <i>et al.</i> , 2019a).	17
Table 2.4	Green synthesis of ZnO nanoparticles using different sources of biological entities with their photocatalytic efficiencies from recent studies.	34
Table 2.5	Influence of metal dopants on photocatalytic activities of ZnO.	40
Table 2.6	Enhanced photocatalytic performances by coupled semiconductors.	43
Table 3.1	Synthesis conditions for optimization of green ZnO synthesis.	56
Table 5.1	Characteristics of MB, CV, and CR dyes (Chen <i>et al.</i> , 2021; Hwang <i>et al.</i> , 2015; Mukhtar <i>et al.</i> , 2021; Wathukarage <i>et al.</i> , 2019).	127
Table 5.2	Comparison of ZnO nanoparticles fabrication using different routes, temperatures, and chemicals.	129
Table 5.3	Comparison of sizes of ZnO nanoparticle synthesized via green and chemical methods with their respective applications.	131
Table 5.4	The S_{BET} , pore volumes, and pore sizes of various ZnO nanoparticles synthesized by green methods.	131
Table 5.5	Comparison of various photocatalysts from recently reported literature for photocatalytic degradation of MB dye.	133
Table 6.1	Thermal stability and char residual weight of NR-PVP, i-NR-PVP/ZnO, and s-NR-PVP/ZnO composite films.	158
Table 7.1	Pseudo-first order and pseudo-second order rate constants and correlation coefficients for the degradation of MB using i-NR-PVP/ZnO and s-NR-PVP/ZnO composite films with various ZnO loadings.	169
Table 7.2	The pseudo-first order rate constants and correlation coefficients for the degradation of MB using i-NR-PVP/ZnO and s-NR-	

	PVP/ZnO composite films under different type and intensity of light irradiation.....	173
Table 7.3	The pseudo-first order rate constants and correlation coefficients for the degradation of MB using i-NR-PVP/ZnO and s-NR-PVP/ZnO composite films under various pH.	177
Table 7.4	The pseudo-first order rate constants and correlation coefficients of trapping experiment.	181
Table 7.5	Kinetic data for photocatalytic removal of CV and CR.....	191
Table 7.6	Comparison of recently reported studies on rubber-based immobilized photocatalysts with the present study.	192

LIST OF FIGURES

	Page
Figure 2.1	Important characteristics of good photocatalysts..... 16
Figure 2.2	Basic steps of photocatalysis (Ong <i>et al.</i> , 2018)..... 19
Figure 2.3	Mechanism of semiconductor photocatalysis (Nunes <i>et al.</i> , 2021). 20
Figure 2.4	Ball-and-stick representations of ZnO crystal structures. (a) cubic rock salt (B1), (b) cubic zinc blende (B3), and (c) hexagonal wurtzite (B4) (Özgür <i>et al.</i> , 2005). 21
Figure 2.5	Preferential ZnO wurtzite crystal growth directions and plausible structures (Leonardi, 2017). 23
Figure 2.6	Morphologies of ZnO with various dimensions. 0D ZnO: (a) quantum dots, (b) nanospheres. 1D ZnO: (c) nanorods, (d) nanowires, (e) nanobelts, (f) nanofibres. 2D ZnO: (g) nanosheets, (h), nanoflakes, (i) disk-like. 3D ZnO: (j) tetrapods, (k) nanoflowers, (l) urchin-like (Arasu <i>et al.</i> , 2019; Kong <i>et al.</i> , 2018; Lee <i>et al.</i> , 2020; Manjula <i>et al.</i> , 2020; Meinderink <i>et al.</i> , 2019; Qu <i>et al.</i> , 2019; Rao <i>et al.</i> , 2019; Saleh, 2019; Sun <i>et al.</i> , 2020; Thakur <i>et al.</i> , 2020; Xu <i>et al.</i> , 2020; Zhu <i>et al.</i> , 2018). 24
Figure 2.7	The principles of green chemistry (Whiteker, 2019). 33
Figure 2.8	The mechanism involved in green synthesis of nanoparticles (Ghosh <i>et al.</i> , 2017). 35
Figure 2.9	The proposed photocatalytic degradation by metal doping (Lee <i>et al.</i> , 2016). 38
Figure 2.10	The proposed photocatalytic degradation by semiconductor coupling (Lee <i>et al.</i> , 2016). 41
Figure 2.11	The chemical structure of NR. 49
Figure 2.12	The chemical structure of PVP. 50
Figure 2.13	Bio-inspired hybrid materials as photocatalysts. 53
Figure 3.1	The (a) photocatalytic setup and its (b) schematic diagram used for the degradation of MB. 65
Figure 3.2	Flow diagram of experimental work involved in the study. 71

Figure 4.1	(a) UV-Vis DRS spectra and (b) band gap energies of biosynthesized ZnO at different pH values (BP extract = 1 mL, $[Zn^{2+}] = 0.02$ M, synthesis time = 2 h, temperature = 60 °C).....	74
Figure 4.2	FTIR spectra of biosynthesized ZnO at different pH (BP extract = 1 mL, $[Zn^{2+}] = 0.02$ M, synthesis time = 2 h, temperature = 60 °C).....	77
Figure 4.3	XRD patterns of biosynthesized ZnO at different pH (BP extract = 1 mL, $[Zn^{2+}] = 0.02$ M, synthesis time = 2 h, temperature = 60 °C).....	78
Figure 4.4	SEM images of ZnO samples prepared at different pH with magnifications of 100000× and 160000× (BP extract = 1 mL, $[Zn^{2+}] = 0.02$ M, synthesis time = 2 h, temperature = 60 °C).....	81
Figure 4.5	PL emission spectra of biosynthesized ZnO at different pH (BP extract = 1 mL, $[Zn^{2+}] = 0.02$ M, synthesis time = 2 h, temperature = 60 °C).....	83
Figure 4.6	(a) Typical UV-Vis spectrum of degradation of MB and (b) the degradation efficiencies of various ZnO prepared at different pH (BP extract = 1 mL, $[Zn^{2+}] = 0.02$ M, synthesis time = 2 h, temperature = 60 °C, pH of MB = 6).....	85
Figure 4.7	UV-Vis DRS spectra of biosynthesized ZnO nanoparticles recorded as a function of amount of BP extract with the respective removal efficiencies (Conditions of ZnO: pH = 12, $[Zn^{2+}] = 0.02$ M, synthesis time = 2 h, temperature = 60 °C).....	87
Figure 4.8	UV-Vis DRS spectra of biosynthesized ZnO nanoparticles recorded as a function of concentration of zinc acetate dihydrate with the respective removal efficiencies (Conditions of ZnO: pH = 12, BP extract = 1 mL, synthesis time = 2 h, temperature = 60 °C).....	88
Figure 4.9	UV-Vis DRS spectra of biosynthesized ZnO nanoparticles recorded as a function of synthesis time with the respective removal efficiencies (Conditions of ZnO: pH = 12, BP extract = 1 mL, $[Zn^{2+}] = 0.02$ M, temperature = 60 °C).	89
Figure 4.10	UV-Vis DRS spectra of biosynthesized ZnO nanoparticles recorded as a function of temperature with the respective removal efficiencies (Conditions of ZnO: pH = 12, BP extract = 1 mL, $[Zn^{2+}] = 0.02$ M, synthesis time = 3 h).....	90
Figure 5.1	Physical appearances of (a) chemically synthesized ZnO and (b) biosynthesized ZnO nanoparticles.	93
Figure 5.2	XRD patterns of biosynthesized and chemically synthesized ZnO nanoparticles.	94

Figure 5.3	FTIR spectra of (a) biosynthesized ZnO, (b) biosynthesized ZnO after 15 months, and (c) chemically synthesized ZnO.....	96
Figure 5.4	SEM images of (a) biosynthesized and (b) chemically synthesized ZnO nanoparticles.	98
Figure 5.5	EDXs and elemental mappings of (a) biosynthesized and (b) chemically synthesized ZnO nanoparticles.....	99
Figure 5.6	(a and b) TEM micrographs and (c) particle size distribution histograms of biosynthesized ZnO nanoparticles.	100
Figure 5.7	(a and b) TEM micrographs and (c) particle size distribution histograms of chemically synthesized ZnO nanoparticles.....	101
Figure 5.8	Nitrogen adsorption-desorption isotherms and pore size distributions (inset) of (a) biosynthesized and (b) chemically synthesized ZnO.....	103
Figure 5.9	DLS measurements of (a) biosynthesized and (b) chemically synthesized ZnO photocatalysts.....	105
Figure 5.10	(a) UV-Vis DRS spectra and (b) band gap energies of biosynthesized and chemically synthesized ZnO photocatalysts.....	107
Figure 5.11	PL emission spectra of ZnO photocatalysts.....	109
Figure 5.12	XPS spectra of ZnO photocatalysts. (a) Survey scan; (b) Zn 2p, (c) O 1s, and (d) C 1s of biosynthesized ZnO; and (e) Zn 2p, (f) O 1s, and (g) C 1s of chemically synthesized ZnO.....	111
Figure 5.13	pH _{pzc} of ZnO photocatalysts.	112
Figure 5.14	Effect of initial dye concentration on the photocatalytic activity of biosynthesized ZnO photocatalyst (20 mg ZnO, unadjusted pH, reaction time = 7 h).	114
Figure 5.15	Effect of catalyst loading on the photocatalytic activity of biosynthesized ZnO photocatalyst ([MB] _o = 2.0 × 10 ⁻⁵ M, unadjusted pH, reaction time = 7 h).....	115
Figure 5.16	Effect of pH and irradiation time on the photocatalytic activity of biosynthesized ZnO photocatalyst ([MB] _o = 2.0 × 10 ⁻⁵ M, 30 mg ZnO, reaction time = 7 h).....	116
Figure 5.17	Schematic interaction of MB molecules and ZnO surface at various pH values.....	117
Figure 5.18	The removal efficiencies of biosynthesized and chemically synthesized ZnO at optimum conditions ([MB] _o = 2.0 × 10 ⁻⁵ M, 30 mg ZnO catalyst, pH 12, 90 min).	118

Figure 5.19	Recyclability of biosynthesized and chemically synthesized ZnO at optimum conditions ($[MB]_0 = 2.0 \times 10^{-5}$ M, 30 mg ZnO catalyst, pH 12, 90 min under visible light).....	120
Figure 5.20	FTIR spectra of biosynthesized ZnO before and after ten cycles of photocatalytic degradation of MB.	121
Figure 5.21	Effect of scavengers on the photocatalytic activity of biosynthesized ZnO photocatalyst.	123
Figure 5.22	Degradation of MB by biosynthesized ZnO in the presence of visible light.....	125
Figure 5.23	The percentage removal for photodegradation of CV and CR.	126
Figure 6.1	Photographs of NR-PVP, i-NR-PVP/ZnO, and s-NR-PVP/ZnO films.	136
Figure 6.2	XRD patterns of (a) i-NR-PVP/ZnO and (b) s-NR-PVP/ZnO composite films. The XRD patterns of ZnO and NR-PVP are also shown in (a) and (b).	138
Figure 6.3	FTIR spectra of (a) i-NR-PVP/ZnO and (b) s-NR-PVP/ZnO composite films. The FTIR spectra of ZnO, PVP, NR, and NR-PVP are also shown in (a) and (b).	140
Figure 6.4	SEM images of (a) ZnO, (b) NR-PVP, (c) i-NR-PVP/ZnO-0.5, (d) i-NR-PVP/ZnO-1, (e) i-NR-PVP/ZnO-2, and (f) i-NR-PVP/ZnO-3 composite films, and (g) EDX spectrum of i-NR-PVP/ZnO-1 film.....	144
Figure 6.5	SEM images of (a) ZnO, (b) NR-PVP, (c) s-NR-PVP/ZnO-0.5, (d) s-NR-PVP/ZnO-1, (e) s-NR-PVP/ZnO-2, and (f) s-NR-PVP/ZnO-3 composite films, and (g) EDX spectrum of s-NR-PVP/ZnO-1 film.....	146
Figure 6.6	UV-Vis DRS spectra of (a) i-NR-PVP/ZnO and (b) s-NR-PVP/ZnO composite films. The UV-Vis DRS spectra of ZnO and NR-PVP are also shown in (a) and (b).....	149
Figure 6.7	Band gap energies of (a) i-NR-PVP/ZnO and (b) s-NR-PVP/ZnO composite films. The band gap energies of ZnO and NR-PVP are also shown in (a) and (b).....	151
Figure 6.8	PL emission spectra of (a) i-NR-PVP/ZnO and (b) s-NR-PVP/ZnO composite films. The PL emission spectra of ZnO and NR-PVP are also shown in (a) and (b).....	153
Figure 6.9	TGA curves of (a) i-NR-PVP/ZnO and (b) s-NR-PVP/ZnO composite films. The TGA curves of ZnO and NR-PVP are also shown in (a) and (b).	155

Figure 6.10	DTG curves of (a) i-NR-PVP/ZnO and (b) s-NR-PVP/ZnO composite films. The DTG curves of ZnO and NR-PVP are also shown in (a) and (b).	157
Figure 6.11	pH _{pzc} of (a) i-NR-PVP/ZnO and (b) s-NR-PVP/ZnO composite films. The pH _{pzc} of ZnO and NR-PVP are also shown in (a) and (b).	159
Figure 7.1	Effect of ZnO loading on the removal of MB using (a) i-NR-PVP/ZnO and (b) s-NR-PVP/ZnO composite films ([MB] ₀ = 2 × 10 ⁻⁵ M, low visible light irradiation, pH 6).	163
Figure 7.2	The interaction between dye molecules and film with (a) more cavities and (b) less cavity.	164
Figure 7.3	(a) Pseudo-first order and (b) pseudo-second order kinetic plots for the removal of MB using i-NR-PVP/ZnO composite films ([MB] ₀ = 2 × 10 ⁻⁵ M, low visible light irradiation, pH 6).	167
Figure 7.4	(a) Pseudo-first order and (b) pseudo-second order kinetic plots for the removal of MB using s-NR-PVP/ZnO composite films ([MB] ₀ = 2 × 10 ⁻⁵ M, low visible light irradiation, pH 6).	168
Figure 7.5	(a) Effect of type and intensity of light and (b) pseudo-first order kinetic plot for the removal of MB using i-NR-PVP/ZnO-1 composite film ([MB] ₀ = 2 × 10 ⁻⁵ M, pH 6).	172
Figure 7.6	(a) Effect of type and intensity of light and (b) pseudo-first order kinetic plot for the removal of MB using s-NR-PVP/ZnO-1 composite film ([MB] ₀ = 2 × 10 ⁻⁵ M, pH 6).	173
Figure 7.7	(a) Effect of pH and (b) pseudo-first order kinetic plot for the degradation of MB using i-NR-PVP/ZnO-1 composite film ([MB] ₀ = 2 × 10 ⁻⁵ M, low visible light irradiation).	176
Figure 7.8	(a) Effect of pH and (b) pseudo-first order kinetic plot for the degradation of MB using s-NR-PVP/ZnO-1 composite film ([MB] ₀ = 2 × 10 ⁻⁵ M, low visible light irradiation).	177
Figure 7.9	(a) The removal efficiencies and (b and c) pseudo-first order kinetic plots for the degradation of MB by i-NR-PVP/ZnO-1 and s-NR-PVP/ZnO-1 films in the presence of various scavenging agents.	180
Figure 7.10	Proposed mechanism for the degradation of MB by i-NR-PVP/ZnO-1 composite film under visible light illumination.	182
Figure 7.11	Proposed mechanism for the degradation of MB by s-NR-PVP/ZnO-1 composite film under visible light illumination.	183
Figure 7.12	The recyclability of i-NR-PVP/ZnO-1 and s-NR-PVP/ZnO-1 composite films at optimum conditions.	187

Figure 7.13	FTIR spectra of (a) i-NR-PVP/ZnO-1 and (b) s-NR-PVP/ZnO-1 films before and after the photocatalytic reactions.	188
Figure 7.14	(a) The percentage removal and (b and c) pseudo-first order kinetic plots for photodegradation of CV and CR by composite films.	190

LIST OF SYMBOLS

%	Percentage
°C	Degree Celsius
$\cdot\text{OH}$	Hydroxyl radical
C_o	Initial dye concentration
C_t	Dye concentration at time t
e^-	Electron
eV	Electron volt
g	Gram
h	Hour
h^+	Hole
$h\nu$	Photon energy
K	Kelvin
k_1	Kinetic rate constant for pseudo-first order
k_2	Kinetic rate constant for pseudo-second order
M	Molar
min	Minute
mL	Milliliter
nm	Nanometer
°	Degree
$\text{O}_2^{\bullet-}$	Superoxide anion radical
O_i	Oxygen interstitial
R^2	Correlation coefficient
S_{BET}	BET specific surface area

T_{\max}	Maximum degradation temperature
T_{onset}	Onset temperature of degradation
V_{O}	Oxygen vacancy
wt%	Weight percent
Zn_i	Zinc interstitial
ZnO	Zinc oxide
θ	Theta
λ	Wavelength

LIST OF ABBREVIATIONS

AA	Ascorbic acid
ACM	Acetaminophen
AOP	Advanced Oxidation Process
ATR	Attenuated total reflectance
BB	Bismarck Brown
BET	Brunauer-Emmett-Teller
BJH	Barrett-Joyner-Halenda
BP	Banana peel
CB	Conduction band
CR	Cresol Red
CRD	Congo Red
CV	Crystal Violet
DB15	Direct Blue 15
DBT	Dibenzothiophene
DF	Diclofenac
DLS	Dynamic light scattering
DTG	Derivative thermogravimetry
EBT	Eriochrome Black-T
EDTA-2Na	Ethylenediaminetetraacetic acid disodium salt dihydrate
EY	Eosin Yellow
FTIR	Fourier Transform Infrared
FWHM	Full width at half maximum
IC	Indigo Carmine

i-NR-PVP/ZnO	Impregnated-natural rubber-polyvinylpyrrolidone/zinc oxide
IPA	Isopropyl alcohol
IUPAC	International Union of Pure and Applied Chemistry
JCPDS	Joint Committee on Powder Diffraction Standards
LF	Levofloxacin
LH	Langmuir-Hinshelwood
MB	Methylene Blue
MG	Malachite Green
MO	Methyl Orange
NAD	Nitrogen adsorption-desorption
NO	Nitric oxide
NR	Natural rubber
NR-PVP	Natural rubber-polyvinylpyrrolidone
NZ	Nizatidine
OG	Orange G
PAM	Polyacrylamide
PAN	Polyacrylonitrile
PANI	Polyaniline
PDI	Polydispersity index
PEG	Polyethylene glycol
pH _{pzc}	Point of zero charge
PL	Photoluminescence spectroscopy
PMMA	Poly(methyl methacrylate)
Ppy	Polypyrrole
PTh	Polythiophene

PVA	Polyvinyl alcohol
PVDF	Poly(vinylidene fluoride)
PVP	Polyvinylpyrrolidone
RhB	Rhodamine B
SEM-EDX	Scanning electron microscopy-energy dispersive X-ray spectroscopy
s-NR-PVP/ZnO	Strewn-natural rubber-polyvinylpyrrolidone/zinc oxide
SPR	Surface Plasmon Resonance
TCH	Tetracycline hydrochloride
TEM	Transmission electron microscopy
TGA	Thermogravimetric analysis
TOC	Total organic carbon
TY	Titan Yellow
TZ	Tartrazine
UV	Ultraviolet
UV-Vis	Ultraviolet-visible
UV-Vis DRS	Ultraviolet-visible diffuse reflectance spectroscopy
VB	Valence band
XPS	X-ray photoelectron spectroscopy
XRD	X-ray diffraction

**FOTOMANGKIN HIJAU BERASASKAN ZINK OKSIDA:
PENYEDIAAN, PENCIRIAN DAN KAJIAN FOTOPEMANGKINAN BAGI
DEGRADASI PEWARNA DI BAWAH SINARAN CAHAYA NAMPAK**

ABSTRAK

Terdapat kekurangan literatur mengenai fabrikasi fotomangkin zink oksida (ZnO) menggunakan laluan biosintetik yang lebih hijau dan bahan berasaskan bio, dengan tumpuan utama untuk meningkatkan kebolegunaan semula, pengumpulan, dan pemulihan fotomangkin. Selain itu, ZnO mengalami kecekapan fotodegradasi yang rendah disebabkan oleh penyerapan cahaya nampak yang rendah dan penggabungan semula pembawa cas fotogenerasi yang tinggi. Dalam kajian ini, fotomangkin hijau berasaskan ZnO telah berjaya disintesis pada suhu bilik menggunakan kaedah mesra alam, kos rendah, dan mudah. Kerja ini menyerlahkan gabungan pengukuhan sisa kulit pisang (BP) dan biopolimer getah asli (NR) untuk membangunkan fotomangkin yang berkesan, ekonomi, dan mampan dengan kebolegunaan semula yang baik untuk penyingkiran pewarna yang tinggi. Fotoaktiviti fotomangkin ini dinilai oleh degradasi pewarna Biru Metilena (MB) di bawah sinaran cahaya nampak. Nanopartikel ZnO pada mulanya disintesis menggunakan ekstrak BP sebagai agen pengurangan dan penyekat. Keadaan terbaik untuk sintesis hijau ZnO ialah pH 12, 1 mL ekstrak BP, 0.02 M zink asetat dihidrat, masa sintesis 3 jam dan suhu 60 °C. ZnO yang dibiosintesis mempamerkan sifat termaju dan prestasi fotopemangkinan yang unggul daripada ZnO yang disintesis secara kimia, yang disediakan untuk tujuan perbandingan. Di bawah keadaan tindak balas optimum (30 mg ZnO, larutan 2.0×10^{-5} M MB, pH 12, 90 minit), ZnO yang dibiosintesis memaparkan 100% penyingkiran MB berbanding 87.7%

penyingkiran yang dicapai oleh ZnO yang disintesis secara kimia. ZnO yang dibiosintesis mengekalkan aktiviti fotopemangkinan yang tinggi dengan empat kitaran berturut-turut manakala ZnO yang disintesis secara kimia hanya mengekalkan tiga kitaran penggunaan lanjutan. Pemisahan dan pengumpulan fotomangkin terampai yang menyusahkan telah diperbetulkan dengan imobilisasi ZnO. ZnO yang dibiosintesis kemudiannya dipegunkan ke dalam dan ke atas filem getah asli-polivinilpirrolidon (NR-PVP) melalui kaedah impregnasi dan bertaburan, membentuk filem komposit getah asli-polivinilpirrolidon/zink oksida-pegun (i-NR-PVP/ZnO) dan getah asli-polyvinylpyrrolidon/zink oksida-bertaburan (s-NR-PVP/ZnO). Walaupun kawasan permukaan dikorbankan disebabkan oleh imobilisasi ZnO, filem menunjukkan degradasi fotopemangkinan yang lebih tinggi daripada ZnO murni pada pH yang hampir neutral. Kecekapan penyingkiran tertinggi untuk degradasi MB oleh filem i-NR-PVP/ZnO dan s-NR-PVP/ZnO dicapai dengan menggunakan 1 wt% ZnO pada pH 6 di bawah 180 minit sinaran cahaya nampak intensiti rendah masing-masing dengan penyingkiran 93% dan 97%. Fotoaktiviti unggul filem s-NR-PVP/ZnO adalah disebabkan oleh kapasiti penyerapan cahaya yang lebih tinggi, penggabungan semula pembawa cas fotogenerasi yang lebih rendah, ketersediaan tapak aktif yang lebih tinggi yang boleh diakses untuk degradasi, dan interaksi permukaan yang lebih baik. Fotodegradasi MB oleh filem komposit mengikut model kinetik tertib pseudo-pertama. Selain itu, kedua-dua filem komposit i-NR-PVP/ZnO dan s-NR-PVP/ZnO mempamerkan kebolegunaan semula yang tinggi masing-masing dengan kecekapan >88% dan >90% selepas sepuluh kitaran degradasi dengan pemisahan selepas rawatan yang mudah. Semua fotomangkin hijau berasaskan ZnO menunjukkan keupayaan untuk memfotodegradasi pewarna anionik dan kationik lain, berfungsi sebagai potensi besar dalam pemulihan alam sekitar untuk rawatan air sisa.

**GREEN ZINC OXIDE-BASED PHOTOCATALYSTS:
PREPARATION, CHARACTERIZATION AND PHOTOCATALYTIC STUDY
FOR THE DEGRADATION OF DYES UNDER VISIBLE LIGHT
IRRADIATION**

ABSTRACT

There is a scarcity of literature on the fabrication of zinc oxide (ZnO) photocatalyst using a greener biosynthetic route and bio-based materials, with a primary focus on improving the reusability, collection, and recovery of the photocatalyst. Besides, ZnO suffers from low photodegradation efficiency due to low visible light absorption and high recombination of photogenerated charge carriers. In this study, green ZnO-based photocatalysts were successfully synthesized at room temperature using environmentally friendly, low cost, and facile methods. The work highlights the combination of valorization of banana peel (BP) waste and natural rubber (NR) biopolymer to develop effective, economic, and sustainable photocatalysts with good reusability for high removal of dyes. The photoactivity of these photocatalysts were evaluated by the degradation of Methylene Blue (MB) dye under visible light irradiation. The ZnO nanoparticles were initially synthesized using BP extract as reducing and capping agents. The best conditions for green synthesis of ZnO were pH 12, 1 mL BP extract, 0.02 M zinc acetate dihydrate, 3 h synthesis time, and 60 °C temperature. The biosynthesized ZnO exhibited advanced properties and superior photocatalytic performance than the chemically synthesized ZnO, which was prepared for comparison purposes. Under optimum reaction conditions (30 mg ZnO, 2.0×10^{-5} M MB solution, pH 12, 90 min), the biosynthesized ZnO displayed 100% removal of

MB as compared to 87.7% removal achieved by the chemically synthesized ZnO. The biosynthesized ZnO sustained high photocatalytic activity over four consecutive cycles whereas the chemically synthesized ZnO only maintained three cycles of extended usage. The inconvenient separation and collection of the suspended photocatalyst were rectified by immobilization of ZnO. The biosynthesized ZnO was subsequently immobilized into and onto the natural rubber-polyvinylpyrrolidone (NR-PVP) film by impregnation and strewn methods, forming the impregnated-natural rubber-polyvinylpyrrolidone/zinc oxide (i-NR-PVP/ZnO) and strewn-natural rubber-polyvinylpyrrolidone/zinc oxide (s-NR-PVP/ZnO) composite films. Despite the sacrificed surface area due to the immobilization of ZnO, the films demonstrated higher photocatalytic degradation than the pristine ZnO at a nearly neutral pH. The highest removal efficiency for the degradation of MB by i-NR-PVP/ZnO and s-NR-PVP/ZnO films were achieved by using 1 wt% of ZnO at pH 6 under 180 min of low intensity visible light exposure with 93% and 97% removal, respectively. The superior photoactivity of s-NR-PVP/ZnO films is due to higher light absorption capacity, lower recombination of photogenerated charge carriers, higher availability of active sites accessible for degradation, and better surface interaction. The photodegradation of MB by the composite films followed the pseudo-first order kinetic model. Moreover, both i-NR-PVP/ZnO and s-NR-PVP/ZnO composite films exhibited high reusability with >88% and >90% efficiency, respectively after ten degradation cycles with convenient post-treatment separation. All green ZnO-based photocatalysts demonstrated capability to photodegrade other anionic and cationic dyes, serving as a great potential in environmental remediation for wastewater treatment.

CHAPTER 1

INTRODUCTION

1.1 Background

Water is a very important resource that all life on the planet relies on for subsistence. At present, the need for this resource continues to increase due to high industrialization and increasing human population growth worldwide. Unfortunately, domestic, industrial, agricultural, clinical, and other activities have led to water contamination, making the availability of clean water challenging. The United Nations projection showed that as much as half to two thirds of the population in the world would face fresh water shortage in 2025 (Barlow and Clarke, 2003). In addition, more than 0.78 billion people worldwide reportedly lack of access to clean water supplies, resulting in severe health issues (Organization and UNICEF., 2013). The accessibility of water sources is critical for human survival in terms of both quality and quantity.

Currently, the detection of dyes as pollutants in water bodies is a worldwide phenomenon. Dyes are extensively used in textile industries and contribute enormously to the environmental pollution. During the dyeing and finishing procedures in the textile industry, up to 200,000 tons of the dyes are lost to effluents each year (Ogugbue and Sawidis, 2011). Majority of the dyes are of synthetic origin which are stable and non-biodegradable due to complex aromatic structures thus make them persist in the water and hard to be eliminated (Sinha *et al.*, 2018). Their presence in water causes catastrophic effects to aquatic organisms and human beings by carcinogenic and mutagenic effects. Diseases concerning to the detrimental effects of dyes has been reported (Manippady *et al.*, 2020; Nor *et al.*, 2015). Massive efforts have been made to minimize the impact of these dyes to the environment. Unfortunately, most water

treatment technologies are incapable to remove the dyes completely from water. Therefore, the search for effective water treatment technologies to remove dyes is of great importance, as the dangerous and toxic pollutants in water could bring malignant effects to living things and cause severe impacts to the environment.

Among the many possible solutions to this problem, photocatalysis emerges as an intriguing approach for the removal of dyes because it is cost-effective, safe, non-toxic, and renewable. Recently, semiconductor-based photocatalyst has gained significant attention since it offers possible solutions to environmental problems. Zinc oxide (ZnO) nanostructures have emerged to be as promising photocatalyst for the removal of pollutants in water owing to their excellent and attractive characteristics. ZnO has the capability in generating reactive oxygen species (Ong *et al.*, 2018) as well as possess a large surface area and exhibits high amount of active sites, which is advantageous in catalysis (Umar *et al.*, 2011a). The amphoteric behavior of ZnO is a unique characteristic that makes it an efficient water remediation technique for the removal of multiple contaminants. Due to its high photosensitivity, bio-safe, low cost, and less-toxic nature, ZnO is therefore considered as an effective photocatalyst for the degradation of organic contaminants in water (Ferreira *et al.*, 2021; Md Rosli *et al.*, 2018; Vaiano *et al.*, 2017).

The immobilization of photocatalyst onto a substrate is effective in rectifying the issues that arise during the application and recovery of powdered photocatalysts from the reaction suspension. Immobilization provides easy separation and recollection, prevents catalyst loss, as well as enables prolonged use of photocatalysts. The integration of nanomaterials with polymer matrices in the form of films has been regarded as a constructive strategy that has garnered considerable attention due to its availability, reliability, low cost, and high stability of the polymer substrates

(Bustamante-Torres *et al.*, 2021). Therefore, the fabrication of polymer-supported photocatalyst is essential to make the photocatalytic degradation of contaminants a convenient and effective operation.

Furthermore, photocatalytic materials derived from biodegradable and renewable resources has become a valuable substitute for the existing materials in water treatment applications and provide a cheaper, sustainable, and environment-friendly solution for dealing with the rising demands of clean water globally for greener sustainable future. The employment of biogenic ZnO nanoparticles and natural polymers is preferable and highly advantageous as they possess distinctive and unique properties that improved the visible-photocatalytic activities towards hazardous dyes. This is a promising option because it is simple, less time consuming, economical, non-toxic, and environmentally benign because bio-based sources are more available and affordable (Saratale *et al.*, 2018). Besides, this approach offers a more sustainable synthetic route which not only helps to preserve the environmental sustainability, but also maximize efficiency and minimize the hazardous effects to both human and environment.

1.2 Problem statements

The presence of hazardous dyes such as Methylene Blue (MB), Crystal Violet (CV), and Cresol Red (CR) in water bodies is a major concern (Marghzari *et al.*, 2018; Wang *et al.*, 2021b). They are exceptionally stable, non-biodegradable, and have complicated aromatic molecular structures which make them hard to be removed. These dyes cause various high potential health risks in humans due to their toxicity, carcinogenic and mutagenic effects. Besides, they also cause adverse effects on the photosynthetic activities of aquatic life by reducing the light penetration hence lead to

oxygen deficiency and deregulates the biological cycles. Therefore, there is a great need to develop a low-cost, effective, and environment-friendly method to treat the dyes for the safety of environment and living things.

Besides TiO₂, ZnO is one of the most promising photocatalysts owing to its low price, green properties, and high photosensitivity. However, despite its versatility, ZnO exhibits low visible light absorption due to its wide band gap energy as well as high recombination rate of photogenerated charge carriers (Güy *et al.*, 2018), which limits its photocatalytic efficacy. Therefore, these issues must be addressed for high photocatalytic performance and for practical applications of ZnO.

In addition, application of photocatalysts in powdered form suffers from a few drawbacks including post-treatment separation process, low reusability, and low light utilization efficiency due to light scattering (Teixeira *et al.*, 2016). Therefore, immobilization of ZnO on support is one of the alternatives to overcome these problems. This approach could reduce the operational cost, simplify the separation procedures, increase recyclability, and prevent complicated recovery of photocatalyst after water treatment, which is attractive for large scale practical applications.

The conventional chemical and physical routes in synthesizing ZnO are expensive, require high energy, employ toxic and harmful chemicals and solvents, as well as generate waste which is hazardous to the environment (Agarwal *et al.*, 2017). In addition, the current methods and substrates used to immobilize ZnO are also costly, toxic, and require special instrumentation, extreme synthesis conditions, and complex procedures. Therefore, fabrication of a more facile, economic, and environmental-friendly photocatalyst using a greener biosynthetic route and bio-based materials is essential to preserve the sustainability of the environment.

1.3 Research objectives

The objectives of this study are:

1. To optimize the synthesis parameters of ZnO nanoparticles prepared by biological method using banana peel (BP) extract as the reducing and capping agents.
2. To evaluate the characteristics and photocatalytic performance of the biosynthesized and chemically synthesized ZnO towards photodegradation of MB under visible light irradiation.
3. To prepare and characterize the impregnated- and strewn-natural rubber-polyvinylpyrrolidone/zinc oxide (i-NR-PVP/ZnO and s-NR-PVP/ZnO) composite films using various techniques.
4. To investigate the potential of i-NR-PVP/ZnO and s-NR-PVP/ZnO composite films towards the degradation of MB under visible light irradiation followed by the optimization of the reaction conditions and kinetics involved during the photocatalytic activities.

1.4 Significance of study

This study highlights the utilization of bio-based materials in the preparation of photocatalysts for sustainable and high removal of dyes under visible light irradiation. The employment of agricultural waste (banana peel (BP)) and biopolymer (natural rubber (NR)) offers a cleaner and greener approach which helps to preserve the sustainability of the environment. The use of eco-friendly natural reducing agent BP extract with ambient synthesis conditions in the preparation of ZnO nanoparticles suggests a more feasible synthetic technique with regards to energy efficiency, waste

prevention, employment of safer solvents and chemicals, and elimination of hazardous substances. It is also one of the various alternatives to convert waste to a more useful application, hence contribute to the sustainability of energy supply while minimizing the impact of waste generation to the environment and preventing pollution.

In addition, the exploitation of renewable and biodegradable resources emanating from biopolymeric materials such as NR is attractive as it helps to keep the operational cost low. The use of non-toxic, easily available, and earth-abundant local material as a support for ZnO is more practical and cost-effective to the water treatment industries and therefore, could serve as a valuable substitute for the existing materials in water treatment applications. Furthermore, the fabrication of bio-benevolent, hybrid photocatalyst from the combination of biosynthesized ZnO and biopolymer matrix is favored and exceptionally advantageous as it possesses high reusability, easier post separation, and versatile properties that enhanced the visible-photocatalytic activities towards organic contaminants. Therefore, the combination of valorization of agricultural waste and renewable biopolymeric material could develop an efficient, sustainable, eco-friendly, and affordable hybrid films for environmental detoxification which fulfils the industrial demands and boost further advancements in greener photocatalytic technologies.

1.5 Scope of study

This study focuses on the fabrication of green ZnO-based photocatalysts using cheap, non-toxic, highly available, and environmental friendly materials as well as facile methods for photocatalytic degradation of MB under visible light irradiation. MB dye was used as the model pollutant throughout this study. The first part deals with the synthesis and optimization of ZnO via green route using BP extract while the second

part is about the immobilization of biosynthesized ZnO into and onto NR polymer matrix by impregnation and strewn methods, respectively. The photocatalysts were characterized using various techniques such as X-ray diffraction (XRD), Fourier transform infrared spectroscopy (FTIR), scanning electron microscopy-energy dispersive X-ray spectroscopy (SEM-EDX), ultraviolet-visible diffuse reflectance spectroscopy (UV-Vis DRS), photoluminescence spectroscopy (PL), transmission electron microscopy (TEM), nitrogen adsorption-desorption (NAD), X-ray photoelectron spectroscopy (XPS), thermogravimetric analysis (TGA), dynamic light scattering (DLS), and point of zero charge (pH_{pzc}). The degradation parameters (effect of initial concentration of MB, ZnO loading, solution pH, irradiation time, and type and intensity of light), recyclability, and applicability of the photocatalysts towards the degradation of other dyes (CV and CR) were also presented. Furthermore, the main reactive species responsible for the degradation of the dyes was also identified and the photocatalytic mechanisms were proposed.

1.6 Thesis outline

This thesis is structured into eight chapters. Chapter 1 provides the general overview of the work, including the problem statements, research objectives, significance and scope of the study, and the outline of thesis. Chapter 2 presents the literature review of the topic. Chapter 3 elaborates the research methodology, which includes the materials and chemicals, methods of synthesis, characterization techniques, and photocatalytic studies procedures. Chapter 4 discusses the green synthesis and optimization of synthesis parameters of ZnO nanoparticles. In Chapter 5, the characterization of structural, morphological, optical, as well as the findings on the photocatalytic studies of optimized biosynthesized ZnO and chemically synthesized

ZnO towards the removal of MB under visible light are compared and discussed. Chapter 6 outlines the fabrication and characterization of the i-NR-PVP/ZnO and s-NR-PVP/ZnO composite films. In Chapter 7, the findings on the photocatalytic studies of the i-NR-PVP/ZnO and s-NR-PVP/ZnO composite films towards the removal of MB under visible light are discussed and compared. Finally, Chapter 8 concludes the major findings of the study and some recommendations for future works are also presented.

CHAPTER 2

LITERATURE REVIEW

2.1 Dyes as organic contaminants

Dyes are colored organic compounds that chemically bond and impart colors to the substrates to which they are being applied. They are usually soluble in water and exist naturally or synthetically. Nowadays, synthetic dyes are primarily used in the textile industries, and they typically originate from coal tar or petroleum-based intermediates (Kumar *et al.*, 2021). Dyes have become one of the major causes of water pollution. According to a report, approximately 7×10^7 tons of dyestuff are produced annually worldwide and 10% of these dyes were discharged to environment as textile effluents after dyeing and processing (Chandanshive *et al.*, 2018). In addition, up to 50% of dyes may not be fixed to the textile fibers during the dyeing process, which were then released into the water bodies (Chaudhari *et al.*, 2017). These large-scale effluents are hazardous and toxic, leading to water contamination and creating health hazards. The release of colored effluents into the environment is detrimental and undesirable, not only due to the mutagenic or carcinogenic dye breakdown products, but also its impact on the aesthetic nature of the environment, water transparency, and gas solubility in the water bodies (Weisburger, 2002). Therefore, it is critical to properly address the dye wastewater treatment in order to avoid endangering human health and polluting the environment as well as for nature preservation.

Dyes exhibit a wide variety of structural diversity and are categorized in various ways. They may be classified according to their chemical structures, solubility, or according to the way they are fixed to the textile fibers (Christie, 2007; Hunger, 2003). Besides, they can also be categorized based on their functional groups or the charge on

the dissociated ions of the dyes in aqueous media which are cationic, anionic, and non-ionic (Yazdani, 2018). The relevance of charges on the dissociated dye molecules and the surface charge of the substrates are two key elements in the treatment of dye wastewater. The major groups of dyes are presented in Table 2.1.

Table 2.1 Classification of dyes (Akbari *et al.*, 2002; Kaykhaii *et al.*, 2018).

Class	Characteristics	Examples	Substrates
Acid	Anionic, water soluble	Acid Red 88, Acid Red 18	Nylon, wool, silk
Basic	Cationic, water soluble	Methylene Blue, Crystal Violet, Safranin	Polyacrylonitrile, polyester, ink, modified nylon
Direct	Anionic, water soluble	Congo Red, Brilliant Blue, Copper Blue 2R	Cotton, rayon, leather, nylon
Disperse	Non-ionic, water insoluble	Disperse Red 1, Disperse Orange 37	Polyester, polyamide, acetate, plastic, acrylic
Reactive	Anionic, water soluble	Reactive Black 5, Reactive Orange 16	Cotton, wool, silk, nylon
Sulfur	Colloidal, water insoluble	Sulfur Brilliant Green, Sulfur Black 1	Cotton, rayon
Vat	Colloidal, water insoluble	Vat Red 10, Vat Orange 1, Vat Violet 13	Cotton, rayon
Solvent	Soluble in organic solvent	Solvent Red 1, Solvent Red 49, Solvent Red 111	Plastics, gasoline, varnishes, lacquers, stains, fats, oil, waxes

Various kind of methods have been employed to remove dyes from wastewater and water resources including chemical, physical, and biological techniques. Physical methods such as sedimentation, adsorption, ion exchange, and filtration are some of the commonly used procedures for wastewater remediation. Adsorption has been widely used because it has simple operation procedures, low cost, and requires less energy and pressure. The drawback of the approach is that no chemical transformation takes place and it only involves the transfer of contaminants from one phase (solution) to another (solid or sludge) without actually destroying them (Pardeshi and Patil, 2008). Although the use of activated carbon adsorption for dye removal is common, the cost of the

treatment may be prohibitively expensive (Malik, 2004). This is due to the additional treatment required for the generated secondary waste, as well as for the regeneration of the inactive adsorbents after use.

Another well-known method for the removal of dyes is the chemical method. The chemical treatment of dyes involves the employment of chemical agents. For instance, coagulants and flocculants like Ca^{2+} , Mg^{2+} , Fe^{3+} , and Al^{3+} are added to wastewater during the coagulation and flocculation processes for detoxification. Previous studies had reported that disperse, vat, and sulfur dyes were significantly removed using these methods (Gao *et al.*, 2007; Hao *et al.*, 2000). However, these techniques produce significant amount of sludge and the cost of treatment is increased due to the employment of the chemicals. Similarly, the use of sodium hypochlorite in the chlorination process assist the disintegration of azo dyes bonding. In most cases, the chlorinated organic compounds by-products are more harmful and carcinogenic than their parent contaminants (Singh *et al.*, 2020). Besides, Advanced Oxidation Processes (AOPs) such as Fenton, electrochemical oxidation, and ozonation are also categorized as chemical methods, which use *in-situ* generated oxidizing agents to degrade contaminants (Samsami *et al.*, 2020). Fenton process suffers from the generation of sludge while electrochemical oxidation requires high operating costs due to high energy consumption (Foo and Hameed, 2010; Sirés *et al.*, 2014). On the other hand, ozonation process produces low amount of sludge, however the method is not desirable due to the employment of strong and non-selective oxidizing agents which is hazardous to the environment (Bizani *et al.*, 2006).

In addition, biological strategies have also been adopted for the detoxification of dyes. The basis of biological method is the utilization of microorganisms for the biodegradation of organic compounds. Fungi and algae are the commonly utilized

microorganisms for the degradation of dyes (Holkar *et al.*, 2016). These microorganisms release enzymes such as laccase, lignin peroxidase, and manganese peroxidase which facilitate the breakdown of dye molecules into non-toxic end products (Holkar *et al.*, 2016). Comparatively to the use of physical and chemical methods, biological methods are more environmentally friendly, generate less sludge, and can degrade and mineralize dyes into less harmful products (Mishra *et al.*, 2021). However, this approach also suffers from several restrictions if applied in large-scale applications. Longer time duration is required for complete removal or mineralization of dyes (Crini, 2006). The poor degradation could be due to the unfavorable environmental conditions as well as the recalcitrant nature and complex molecular structure of the dyes (Claus *et al.*, 2002). Approximately 53% of the dyes are resistant to microbial attack (Vinu *et al.*, 2010). Furthermore, since a large area and high operational cost are needed for treatment plant installation, it is challenging to establish the operational design of the entire system for the application at large scale (Bhattacharyya and Sarma, 2003; Raouf *et al.*, 2019).

The benefits and drawbacks of the various dye wastewater treatment techniques are summarized in Table 2.2. It can be concluded that each of these methods comes with their own set of benefits and drawbacks. However, none of them was able to completely remove the dyes from wastewater. Therefore, it is crucial to look into other effective technique for complete removal of toxic dyes from water. A more competent and sustainable method is paramount for water remediation to meet the global challenges without endangering the environment and living things. Photocatalysis has recently attracted the attention of scientists as an attractive, efficient, and promising alternative to existing technologies for eliminating toxic organic contaminants from water.

Table 2.2 The advantages and disadvantages of various treatment technologies for dye removal from water (Solayman *et al.*, 2023; Srivatsav *et al.*, 2020).

Treatment methods	Advantages	Disadvantages
Adsorption	<ul style="list-style-type: none"> ▪ Simple operation procedure ▪ Requires less energy and pressure ▪ Highly efficient process ▪ Applicable to various target contaminants 	<ul style="list-style-type: none"> ▪ Regeneration of adsorbent material is expensive ▪ Adsorbent performance degrades after multiple operational cycles
Ion exchange	<ul style="list-style-type: none"> ▪ High regeneration of materials ▪ Convenient operation ▪ No sludge production 	<ul style="list-style-type: none"> ▪ High cost ▪ Highly sensitive to pH
Coagulation and flocculation	<ul style="list-style-type: none"> ▪ Easy operation ▪ Effective in removing bacteria, protozoa, and virus 	<ul style="list-style-type: none"> ▪ High operational cost ▪ Produces significant amount of sludge ▪ Large consumption of chemicals
Chlorination	<ul style="list-style-type: none"> ▪ Economical ▪ High water solubility ▪ Toxic to pathogens 	<ul style="list-style-type: none"> ▪ Harmful by-products formation ▪ Very corrosive ▪ Residual toxicity of the effluents
Fenton process	<ul style="list-style-type: none"> ▪ Simple and efficient ▪ Suitable for batch treatment ▪ Decolorization of the effluents 	<ul style="list-style-type: none"> ▪ Suffers from the generation of sludge ▪ Operation in acidic conditions
Ozonation	<ul style="list-style-type: none"> ▪ Produces low amount of sludge ▪ Rapid reaction rate 	<ul style="list-style-type: none"> ▪ High energy demand ▪ High capital cost
Electrochemical oxidation	<ul style="list-style-type: none"> ▪ Rapid process ▪ Low sludge generation ▪ No pH restriction 	<ul style="list-style-type: none"> ▪ Electrode fouling ▪ High operating cost ▪ High energy consumption
Biological treatment	<ul style="list-style-type: none"> ▪ Economically attractive ▪ Environmentally friendly 	<ul style="list-style-type: none"> ▪ Slow process ▪ Biological sludge generation ▪ Requires optimal favorable environment ▪ Requires high maintenance and large area

2.2 Fundamental of heterogenous photocatalysis

Currently, semiconductor heterogeneous photocatalysis, a green technology based on AOP is gaining recognition as an efficient wastewater remediation technique capable of degrading a broad variety of recalcitrant pollutants including dyes. It is one of the advanced physicochemical processes applicable in the photodegradation of environmental organic pollutants present in both water and air (Escobedo and de Lasa, 2020). Photocatalysis has emerged as the best alternative to replace the conventional wastewater purification technology due to its ability to directly utilize light energy for achieving chemical detoxification. Photocatalysis is favored for being energy saving, produces non-toxic compounds and less secondary contaminants, requires mild reaction conditions, and is capable in removing a wide range of pollutants from various media (Al-Nuaim *et al.*, 2022; Buchanan *et al.*, 2005; Kabra *et al.*, 2004). Photocatalysis is effective in mineralizing highly stable organic contaminants such as coloring materials (Suresh and Sivasamy, 2020; Yulizar *et al.*, 2020), phenolic compounds (Liang *et al.*, 2020a; Shen *et al.*, 2019), surfactants (Eng *et al.*, 2010; Kuźmiński *et al.*, 2018), pesticides (Truc *et al.*, 2019; Yadav *et al.*, 2019), as well as some inorganic pollutants (Bao *et al.*, 2019; Shukor *et al.*, 2019) that are resistant to degradation. Apart from removing chemical contaminants, photocatalysis has the potential to inactivate microbes (Reddy *et al.*, 2017; Rodríguez-González *et al.*, 2020) such as bacteria, protozoa, spores, and viruses, which makes it attractive for overall treatment of water. Furthermore, photocatalysis also possesses several other advantages such as rapid degradation rate, reduces the toxicity of organic compounds, and the ability to operate under ambient temperature and pressure (Ong *et al.*, 2018).

2.2.1 Photocatalyst and its characteristics

Photocatalysts are materials or substances that are capable to absorb energy in the form of light to accelerate a photoreaction without being consumed (Umar and Aziz, 2013). The phenomenon that occurs when a light source interferes with the surface of photocatalyst is called as photocatalysis. It is a simple process where two simultaneous reactions which are oxidation and reduction from the photogenerated holes (h^+) and photogenerated electrons (e^-) respectively, take place. These charge-carrier pairs produce potent oxidizing agents that break down and disintegrate organic matters to carbon dioxide (CO_2) and water (H_2O) (Tahir *et al.*, 2020). Several sources of lights such as ultra-violet (UV), visible, artificial, and sunlight can be employed for photocatalyst activation. One of the greatest benefits of photocatalysis is almost all inorganic and organic contaminants can be degraded and mineralized rapidly and effectively by this process at ambient conditions (Bhatkhande *et al.*, 2002).

The photocatalytic efficiency of a photocatalyst is highly dependent on the band gap energy, its well-defined electronic configuration, and the ability to generate electron-hole pairs to produce free radicals. To enhance the effectiveness and economic viability of photocatalysts, the band gap energy should be designed in such a way that the light absorption is extended into the visible region of the light to harness the light energy efficiently. Apart from having an appropriate band gap energy, a photocatalyst is also chosen based on other characteristics such as its less toxic nature, low cost, availability, large surface area, as well as physical and chemical stabilities (Pirhashemi *et al.*, 2018). In addition, a good photocatalyst should also be competent and reliable under various reaction conditions, photocorrosion resistant, and capable to work effectively on frequent or long-term use. Figure 2.1 summarizes the vital features of an excellent photocatalyst.

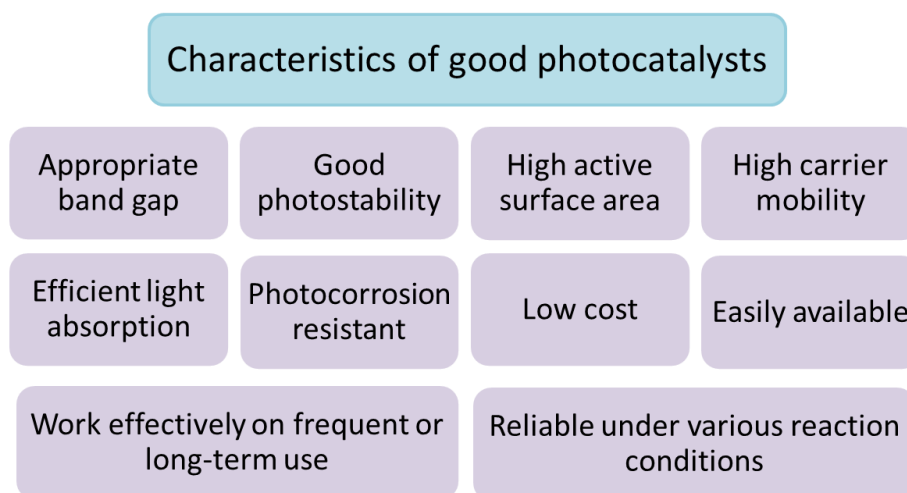


Figure 2.1 Important characteristics of good photocatalysts.

2.2.2 Metal oxide semiconductor photocatalyst

Semiconductor materials are usually regarded as photocatalysts. Currently, over 150 semiconductor materials have been explored for the detoxification of environmental system, comprising of metal oxides, hydroxides, halides, sulfides, carbides, chalcogenides, and oxyhalides (Jayaraman *et al.*, 2015; Theerthagiri *et al.*, 2014). The most promising and widely used semiconductor photocatalysts are metal oxides such as ZnO, Fe₂O₃, TiO₂, SnO₂, ZrO₂, NiO₂, WO₃, CeO₂, and V₂O₅, owing to their effective pollutant removal nature. Oxide-based semiconductor photocatalysts are preferred as they possess extraordinary characteristics with many significant benefits. They exhibit size-tunable properties, large specific surface area, broad absorption spectra with high absorption coefficients, useful optical band gap, and strong oxidizing power (Karthikeyan *et al.*, 2020). They can also afford multiple electron transfer process with extended application without significant loss of photocatalytic activities, stable, cost-effective, and is functional at ambient temperature and pressure (Banerjee *et al.*, 2014). Furthermore, metal oxide semiconductors are known to demonstrate potential in diverse applications such as biomedicine, solar cells, detectors, radiation attenuators,

optoelectronics, energy conversion, and sensors (Abu-Dief, 2020; Chavali and Nikolova, 2019; Ficai *et al.*, 2014; Rashad *et al.*, 2020). They are also heavily employed for water splitting for hydrogen production, carbon dioxide reduction, odor control, as well as cell wall inactivation of bacteria and cancer cells (Husni *et al.*, 2018; Shen *et al.*, 2017; Sirelkhatim *et al.*, 2015; Suanlim *et al.*, 2016). Table 2.3 presents some examples of semiconductor photocatalysts with their band gap energies.

Table 2.3 The band gap energies of various semiconductor photocatalysts (Karthikeyan *et al.*, 2020; Zhang *et al.*, 2019a).

Semiconductor	Band gap energy (eV)
ZnO	3.3
TiO ₂ (anatase)	3.2
TiO ₂ (rutile)	3.0
CuO	2.0
Fe ₂ O ₃	2.2
Bi ₂ O ₃	2.8
WO ₃	2.8
SnO ₂	3.8
V ₂ O ₅	2.7
SrTiO ₃	3.4
ZnS	3.6
CdS	2.4

Among these semiconductor photocatalysts, ZnO has been extensively explored. ZnO is known to possess impressive optical, electronic, catalytic, photochemical, antifouling, antibacterial, and biological properties (Al-Fori *et al.*, 2014; Gharoy Ahangar *et al.*, 2015; Sirelkhatim *et al.*, 2015). ZnO exhibits higher absorption efficiency over a wide fraction of the solar spectrum than TiO₂ (Ong *et al.*, 2018) and the cost of production of ZnO is about 75% lower than those of Al₂O₃ and TiO₂ nanoparticles (Liang *et al.*, 2012). In recent years, ZnO has emerged as a strong

competitor to TiO₂ in wastewater treatment (Udom *et al.*, 2013). ZnO was discovered to exhibit superior photocatalytic activity than TiO₂, particularly in dye-polluted aqueous solutions (Cambrussi *et al.*, 2019; Chantes *et al.*, 2015; Kouhail *et al.*, 2020). Both ZnO and TiO₂ have been employed for photocatalytic degradation of Acid Yellow 73 and Basic Yellow 2 under UV light irradiation, and the ZnO displayed higher percentage removal and degradation rate constant than TiO₂ (Cambrussi *et al.*, 2019). Similar results were also obtained for the removal of Methyl Orange (MO) and Reactive Bezactiv Yellow dyes under sunlight exposure (Kouhail *et al.*, 2020). Besides, ZnO has a substantially higher electron mobility, which is at least two orders of magnitude higher than TiO₂ (Aggelopoulos *et al.*, 2017; Štrbac *et al.*, 2018). Furthermore, ZnO is more versatile than TiO₂ in terms of synthesis and morphologies (Quintana *et al.*, 2007). ZnO nanostructures could be prepared using a variety of synthetic routes with different sizes and morphologies (Shahzad *et al.*, 2021). Thus, ZnO with desired design and shape could be fabricated according to the applications. Additionally, in comparison to TiO₂, ZnO is a preferable alternative since it has more point defects primarily from oxygen vacancies, produces more hydroxyl radicals, and has a faster response rate (Udom *et al.*, 2013). The amphoteric nature of ZnO also makes it a promising photocatalyst.

2.2.3 Principle and mechanism of photocatalysis

The mechanism of photocatalysis involves a chain of processes which can be explained by five simple steps (Molinari *et al.*, 2020) as illustrated in Figure 2.2:

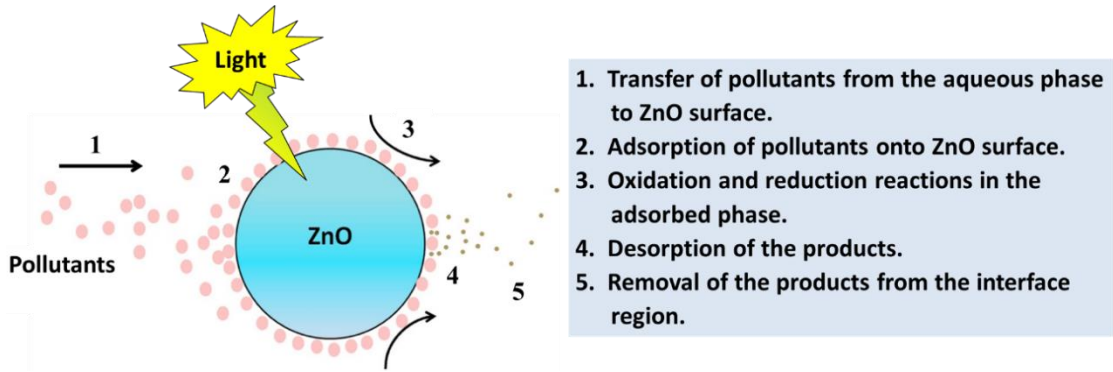
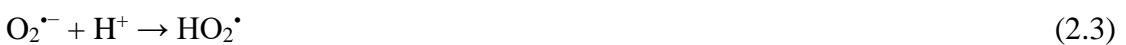
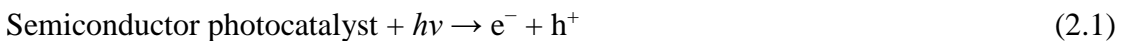


Figure 2.2 Basic steps of photocatalysis (Ong *et al.*, 2018).

When semiconductor photocatalyst is illuminated by light energy ($h\nu$) that is equal to or greater than its band gap energy, the electrons (e^-) from the valence band (VB) are photoexcited and promoted to the conduction band (CB), leaving behind an unfilled space in the VB which is referred to as a hole (h^+). Afterwards, the generated electron-hole pairs migrate to the photocatalyst surface and participate in the oxidation and reduction reactions. As the reactions proceed, superoxide anion radicals ($O_2^{\bullet-}$) and hydroxyl radicals ($\bullet OH$) are produced. The e^- in the CB reacts with oxygen (O_2) to produce $O_2^{\bullet-}$ which is then undergo multiple reactions, subsequently leads to the formation of $\bullet OH$ radicals. The h^+ in the VB on the other hand reacts with H_2O or hydroxyl ions (OH^-) to generate $\bullet OH$ radicals. These powerful oxidizing agents then reduce the pollutants into intermediate compounds or less harmful species such as H_2O and CO_2 . The general mechanism of photocatalysis is illustrated in Figure 2.3 and summarized as follows (Curri *et al.*, 2003):



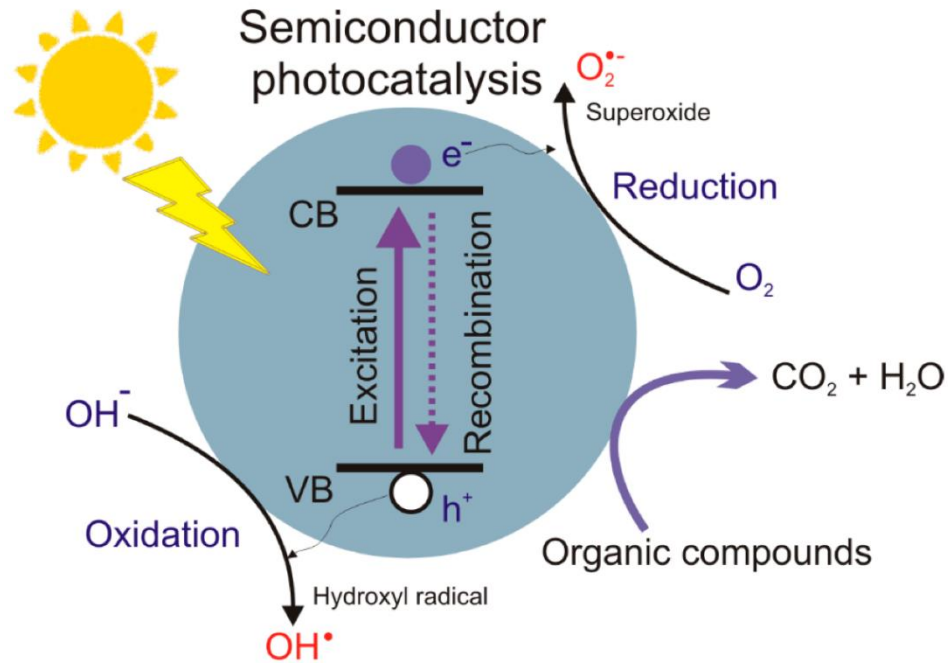
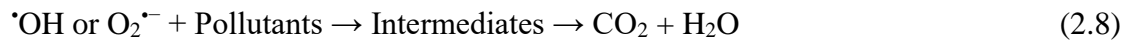


Figure 2.3 Mechanism of semiconductor photocatalysis (Nunes *et al.*, 2021).

2.3 Properties and features of zinc oxide (ZnO)

2.3.1 ZnO structure and classification

ZnO is an inorganic compound that occurs naturally as the rare mineral zincite. It exists as three well-defined crystals namely cubic zinc blende, hexagonal wurtzite, and cubic rock salt lattices. The wurtzite is the most common structure of ZnO while zinc blende and rock salt are occasionally noticed (Dubbaka, 2008; Özgür *et al.*, 2005). The later structures are metastable and rare as they can only be formed under certain conditions such as special controlled growth techniques on cubic substrates and high pressure conditions (Lam *et al.*, 2012). The hexagonal wurtzite phase exhibits the

greatest thermodynamic stability amongst all and is the most stable at ambient pressure and temperature. Therefore, ZnO has a higher propensity to crystallize in wurtzite form, resulting in almost all photocatalytic studies concentrating on photocatalytic properties of this structure. Figure 2.4 depicts the ball-and-stick representations of ZnO crystalline structures, where the yellow and blue spheres represent Zn and O atoms, respectively. The crystallographic structure is a vital property of nanomaterials as it can influence the behavior of the materials. Important physicochemical properties of ZnO such as the band structure and optical transparency are determined by the arrangement of atoms or molecules in a crystalline material (Tudose *et al.*, 2019).

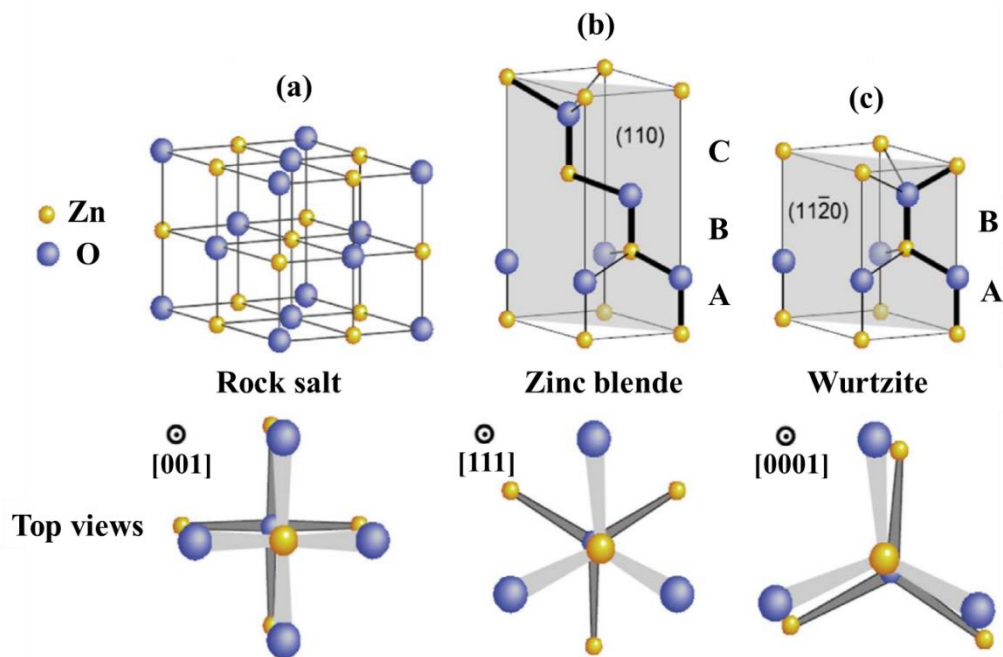


Figure 2.4 Ball-and-stick representations of ZnO crystal structures. (a) cubic rock salt (B1), (b) cubic zinc blende (B3), and (c) hexagonal wurtzite (B4) (Özgür *et al.*, 2005).

The hexagonal wurtzite structure possesses two lattice parameters a and c , with 0.3296 and 0.52065 nm, respectively (Baruah and Dutta, 2009). The wurtzite ZnO is usually illustrated schematically as a number of planes of Zn^{2+} and O^{2-} ions stacked

alternately alongside the c -axis in orderly orientations as hexagonal sublattice patterns. Each sublattice consists of four Zn^{2+} ions and encircled by four O^{2-} ions and vice versa, aligned at the tetrahedron edges (George *et al.*, 2010). The polar symmetry formed along the hexagonal axis rises from this tetrahedral coordination and causes spontaneous polarization in the ZnO (Hughes and Wang, 2004; Kong and Wang, 2003), which plays a key role in the growth of crystals during the synthesis of ZnO nanostructures. The non-centrosymmetric structure causes ZnO to be piezoelectric and pyroelectric due to the lack of inversion core of space groups in ZnO (Maggard *et al.*, 2001; Moore and Wang, 2006). The common polar surfaces of ZnO are the positively charged Zn-(0001) and negatively charged O-(0001) whereas ZnO $(0\ 1\ \bar{1}\ 0)$ and $(2\ \bar{1}\ \bar{1}\ 0)$ facets are the non-polar surfaces with several Zn and O atoms and lower energy level (Sheikh *et al.*, 2019). Studies on the polarity of ZnO nanomaterials are useful for water remediation applications especially photocatalysis to further improve the removal of pollutants under light irradiation. This can be attained by controlling the agglomeration rate of ZnO nanoparticles and increase the positive and negative sites of photocatalyst by tuning its polarity.

ZnO nanostructures can be categorized into zero dimensional (0D), one dimensional (1D), two dimensional (2D), and three dimensional (3D) (Figure 2.5). The formation of ZnO nanostructures is influenced by the variety of synthesis strategies and the kinetics of the synthesis processes (Mishra and Adelung, 2018). Quantum dots (Park *et al.*, 2019; Yuan *et al.*, 2020b) and hollow nanospheres (Alexander *et al.*, 2019; Saleh, 2019) are examples of morphologies of 0D ZnO arrays whereas 1D arrays comprise of nanofibers (Thakur *et al.*, 2020; Thangavel *et al.*, 2020), nanorods (Kumar *et al.*, 2020c; Rajamanickam *et al.*, 2020), nanoneedles (Cha *et al.*, 2018; Gonzalez-Chavarri *et al.*,

2018), nanotubes (Choi and Chang, 2018; Samadipakchin *et al.*, 2017), nanobelts (Kennedy *et al.*, 2018; Rao *et al.*, 2019), and nanowires (Ahmad *et al.*, 2020; Kong *et al.*, 2018). The 2D nanoarchitectures are typically nanosheets (Manjula *et al.*, 2020; Zhang *et al.*, 2020b), nanoflakes (Kanaparthi and Singh, 2020; Khara and Chand, 2019; Kumar *et al.*, 2020b), and disk-like structures (Wang *et al.*, 2016a; Zhu *et al.*, 2018). Examples of ZnO nanostructures in 3D arrays are nanoflowers (Borbón *et al.*, 2019; Qu *et al.*, 2019), urchin-like structures (Le *et al.*, 2017; Wang *et al.*, 2016b), and nanotetrapods (Mishra and Adelung, 2018; Paulowicz *et al.*, 2018). Figure 2.6 presents the morphologies of ZnO with various dimensions. These morphologies influence the physical, optical, electrical, and mechanical properties of ZnO significantly for multiple applications in various fields. Therefore, suitable ZnO nanostructure designs for photocatalytic reactions is required to ensure efficient photocatalytic performances.

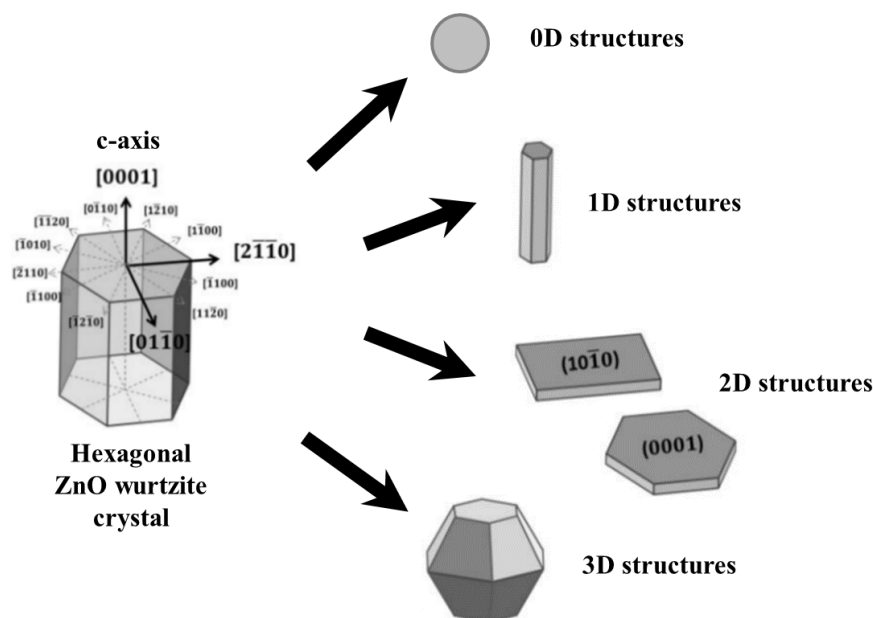


Figure 2.5 Preferential ZnO wurtzite crystal growth directions and plausible structures (Leonardi, 2017).

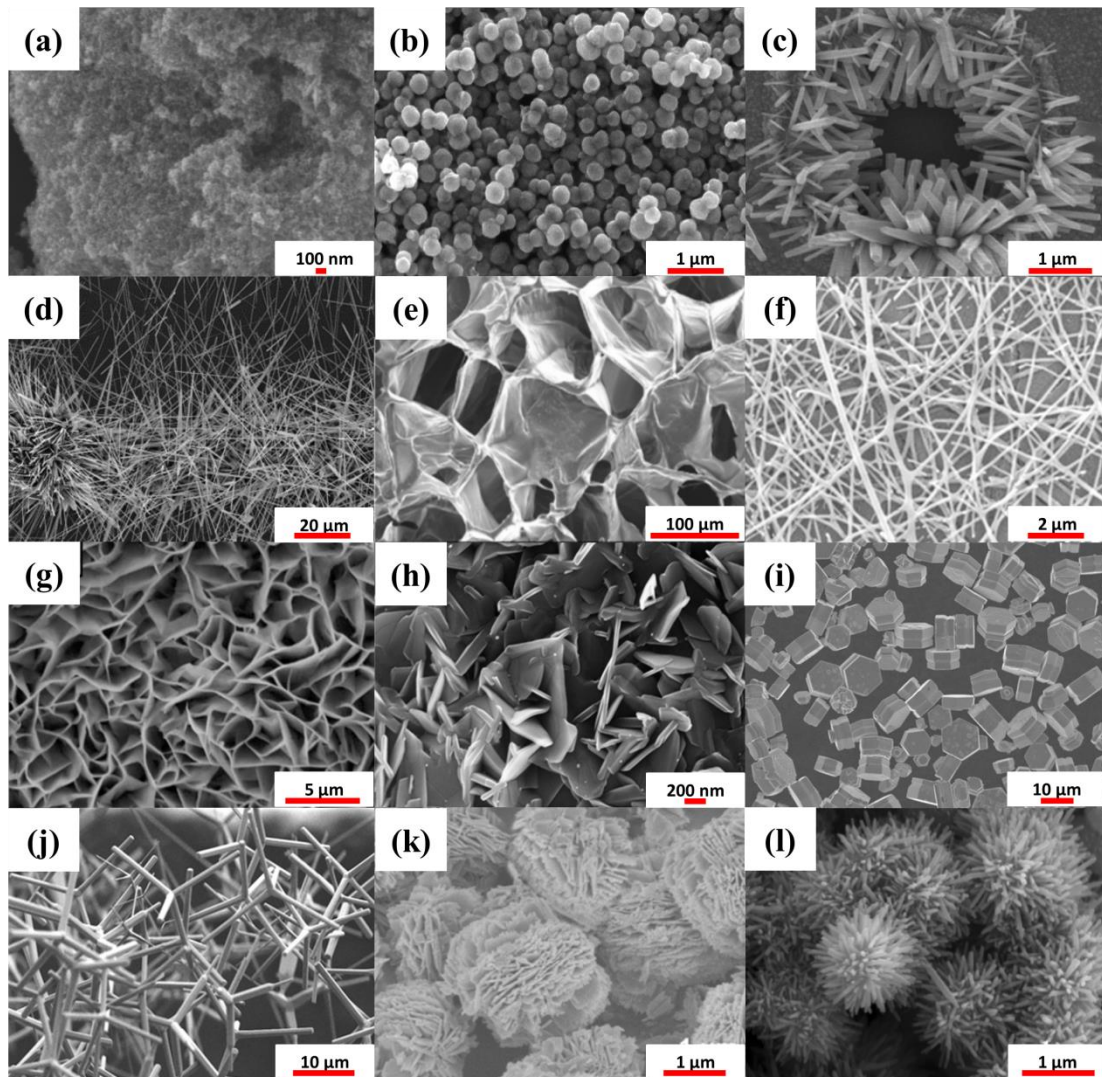


Figure 2.6 Morphologies of ZnO with various dimensions. 0D ZnO: (a) quantum dots, (b) nanospheres. 1D ZnO: (c) nanorods, (d) nanowires, (e) nanobelts, (f) nanofibres. 2D ZnO: (g) nanosheets, (h), nanoflakes, (i) disk-like. 3D ZnO: (j) tetrapods, (k) nanoflowers, (l) urchin-like (Arasu *et al.*, 2019; Kong *et al.*, 2018; Lee *et al.*, 2020; Manjula *et al.*, 2020; Meinderink *et al.*, 2019; Qu *et al.*, 2019; Rao *et al.*, 2019; Saleh, 2019; Sun *et al.*, 2020; Thakur *et al.*, 2020; Xu *et al.*, 2020; Zhu *et al.*, 2018).

It has been reported that ZnO nanoflowers show higher photocatalytic efficiencies than ZnO nanorods (Bourfaa *et al.*, 2020; Son *et al.*, 2018). The 3D structure of ZnO nanoflowers enhance the surface reaction by providing more adsorption sites due to its large surface area for better charge transfer and carrier mobility, thus improve the photoactivity (Shende *et al.*, 2018). In addition, 1D ZnO nanomaterials have